nature chemistry

ARTICLES

PUBLISHED ONLINE: 28 MARCH 2016 | DOI: 10.1038/NCHEM.2491

Experimental realization of two-dimensional boron sheets

Baojie Feng[1], Jin Zhang[1], Qing Zhong[1], Wenbin Li[1], Shuai Li[1], Hui Li[1]*, Peng Cheng[1], Sheng Meng[1,2], Lan Chen[1]* and Kehui Wu[1,2]*

A variety of two-dimensional materials have been reported in recent years, yet single-element systems such as graphene and black phosphorus have remained rare. Boron analogues have been predicted, as boron atoms possess a short covalent radius and the flexibility to adopt sp^2 hybridization, features that favour the formation of two-dimensional allotropes, and one example of such a borophene material has been reported recently. Here, we present a parallel experimental work showing that two-dimensional boron sheets can be grown epitaxially on a Ag(111) substrate. Two types of boron sheet, a β_{12} sheet and a χ_3 sheet, both exhibiting a triangular lattice but with different arrangements of periodic holes, are observed by scanning tunnelling microscopy. Density functional theory simulations agree well with experiments, and indicate that both sheets are planar without obvious vertical undulations. The boron sheets are quite inert to oxidization and interact only weakly with their substrate. We envisage that such boron sheets may find applications in electronic devices in the future.

Boron is the fifth element in the periodic table and has a rich chemistry that is second only to carbon[1–3]. A striking feature of boron is that B_{12} icosahedral cages occur as the building blocks in bulk boron and many boron compounds[2,3]. This differs from its neighbouring element, carbon, which prefers a two-dimensional (2D) layered structure (graphite) in its bulk form. Meanwhile, boron clusters of medium size have been predicted to be planar or quasi-planar, for example, B_{12}^-, B_{13}^+, B_{19}^- and B_{36} (refs 4–10). This is also in contrast to carbon clusters, which exhibit various cage structures (fullerenes). Now, with the boom in graphene research, an intriguing question is whether boron can also form a monoatomic-layer 2D sheet structure? Here, we report the realization of 2D boron sheets by molecular beam epitaxy. Two types of boron sheet, consisting of a triangular boron lattice with different arrangements of hexagonal holes, have been identified. An X-ray photoelectron spectroscopy (XPS) study indicated that the 2D boron sheets are quite stable against oxidization, suggesting that they merit future investigation for potential applications.

Graphene is the building block in a number of carbon nanostructures, including fullerenes and nanotubes[11,12]. Boron has the same short covalent radius and the flexibility to adopt sp^2 hybridization as carbon, which would favour the formation of various low-dimensional allotropes, such as boron nanotubes, fullerenes and 2D boron sheets[13–15]. The 2D boron structure is particularly interesting as it has been predicted to be metallic[16–20], despite bulk boron being a semiconductor. In fact, compound MgB_2, which consists of alternative boron and magnesium layers, exhibits high-T_c superconductivity[21]. Some 2D boron structures have recently been predicted to host Dirac fermions[22]. Theoretically, a large variety of planar 2D boron structures with competitive cohesive energy, such as α sheets[16,17], β sheets[16,17] and χ sheets[19,20], named after the connectivity of the boron, have been predicted. However, the experimental realization of 2D boron sheets remains a challenge. Recently, it was suggested that 2D boron sheets can form on metal substrates, such as Cu(111)[23], Ag(111) and Au(111)[24], due to the stabilization of sp^2 hybridization by metal passivation. Following this idea, we used molecular beam epitaxy (MBE) to grow boron sheets on a Ag(111) surface in ultrahigh vacuum (UHV) and successfully obtained 2D boron sheets, in a manner similar to those recently reported in a parallel work by A. J. Mannix *et al.*, referred to as 'borophene' in analogy with graphene[25].

Results and discussion

Growth of 2D boron. Boron was grown on a single-crystal Ag(111) surface by direct evaporation of a pure boron source. When the substrate temperature during growth was below 500 K, we found only clusters or disordered structures on the surface (Supplementary Fig. 1a). At a temperature of ~570 K, monolayer (ML) islands with a perfectly ordered structure form on the surface, as shown in Fig. 1a. The scanning tunnelling microscope (STM) image with high contrast in Fig. 1b shows parallel stripes on the island surface in the $[\bar{1}10]$ direction of Ag(111). The separation between stripes is 1.5 nm (indicated by the solid lines in Fig. 1b). The high-resolution STM image in Fig. 1c reveals ordered, parallel rows of protrusions along the $[\bar{1}12]$ direction of the Ag(111) substrate (horizontal direction in Fig. 1c). The distance between nearest-neighbour protrusions is 3.0 Å along the rows and 5.0 Å across the rows, respectively (marked by the black rectangle). The 1.5 nm stripes observed in large-scale images (black lines in Fig. 1b) correspond to the slightly brighter protrusions, which are aligned in the direction perpendicular to the rows, as marked by the lines in Fig. 1c. This phase is labelled 'S1'.

By annealing the sample to 650 K, we observed the transition of the S1 phase to another ordered structure (labelled 'S2'), as shown in Fig. 1d. The S2 phase usually coexists with the S1 phase in the temperature range from 650 to 800 K. At higher temperatures, most areas of the surface will be transformed to the S2 phase. The S2 phase can also be obtained by directly growing boron on Ag(111) with a substrate temperature of ~680 K (Supplementary Fig. 1c). The high-resolution STM images in Fig. 1e,f show that the S2 phase also consists of parallel rows of protrusions in the $[\bar{1}12]$ direction

[1]Institute of Physics, Chinese Academy of Sciences, Beijing 100190, China. [2]Collaborative Innovation Center of Quantum Matter, Beijing 100871, China. *e-mail: huili8@iphy.ac.cn; lchen@iphy.ac.cn; khwu@iphy.ac.cn

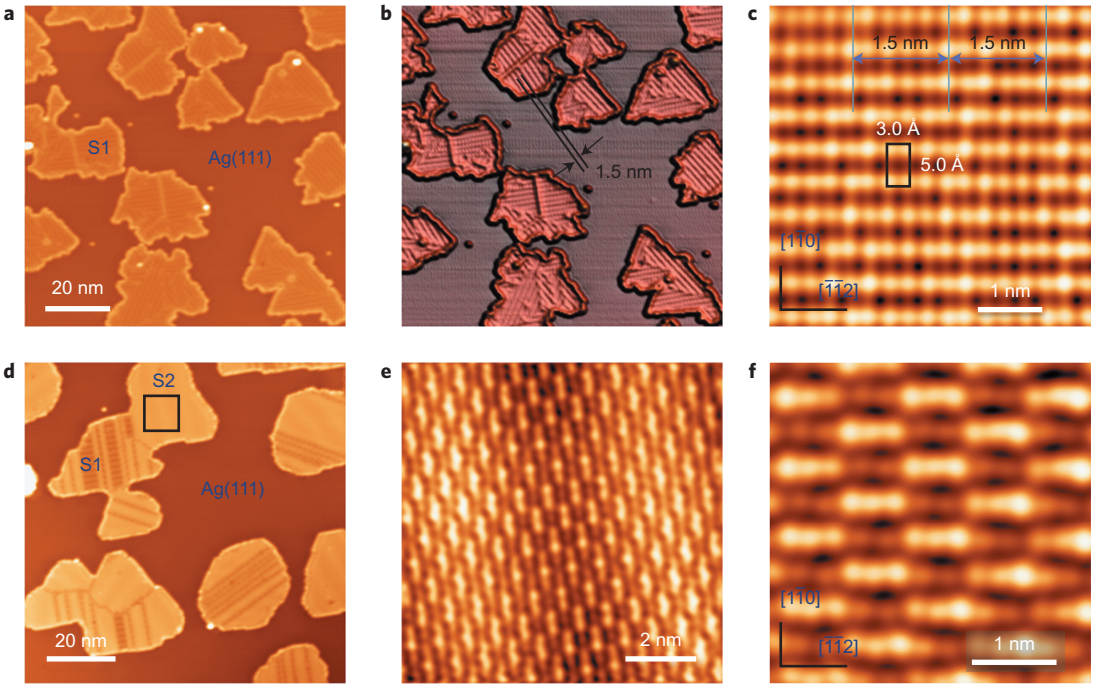

Figure 1 | Formation of 2D boron sheets on Ag(111). a, STM topographic image of boron structures on Ag(111), with a substrate temperature of ~570 K during growth. The boron islands are labelled as 'S1' phase. **b**, Three-dimensional version of **a**, in which the stripes with 1.5 nm intervals are clearly resolved. **c**, High-resolution STM image of S1 phases. The S1 unit cell is marked by a black rectangle, and the 1.5 nm stripes are indicated by solid lines. **d**, STM image of boron sheets after annealing the surface in **a** to 650 K. The two different phases are labelled 'S1' and 'S2'. Most boron islands are transformed to the S2 phase, but the S1 phase still remains in small parts of the islands. **e**, STM image obtained on the area marked by the black rectangle in **d**. **f**, High-resolution STM image of the S2 phase, zoomed from **e**. Note that the orientation of the image is rotated to allow comparison with **c**. Bias voltages of STM images: –4.0 V (**a**,**b**), 0.9 V (**c**), –4.0 V (**d**), 1.0 V (**e**,**f**).

of the Ag(111) substrate. The distance between nearest-neighbour protrusions is 3.0 Å along the rows, and 4.3 Å across the rows. Another obvious feature is that the protrusions along the rows are divided into sections with alternate brighter and darker protrusions. Each section comprises five protrusions, so the periodicity along the row is 3.0 Å × 5 = 1.5 nm.

Structures of 2D boron. As boron has very low solubility in bulk silver, we first assume that both of these structures are pure boron sheets. Among a large number of planar boron monolayer models in the literature, we find that the β_{12} sheet structure[20] agrees very well with the S1 phase. In fact, the β_{12} sheet was predicted to form on a Ag(111) substrate in a recent, independent theoretical study[26]. The β_{12} sheet model is characterized by hole chains separated by hexagonal boron rows. Its unit cell is rectangular, with lattice constants of 3.0 and 5.0 Å in the two directions. To confirm this model, we performed first-principles calculations on the β_{12} sheet involving the Ag(111) substrate. The β_{12} sheet was placed on Ag(111) with the boron rows in the [$\bar{1}$12] direction of the Ag(111) surface, as shown in Fig. 2a. After relaxation, the global structure of the β_{12} sheet remains planar. It is noted that, due to the lattice mismatch, five times the lattice constant of the boron sheet along the rows (3.0 Å × 5 = 15.0 Å) fits well with three times the period of Ag(111) (3 × 2.9 Å × $\sqrt{3}$ = 15.06 Å). This means that a Moiré pattern with 1.5 nm periodicity will form along the boron row direction, which explains the 1.5 nm stripes observed in the STM image (Fig. 1c). The simulated STM image of the β_{12} sheet on Ag(111) shown in Fig. 2c reproduces both the rectangular lattice and the parallel striped patterns, in agreement with the STM images.

On the other hand, the S2 phase most probably corresponds to the χ_3 sheet model in the literature[20], as shown in Fig. 2d. The structure of the χ_3 sheet consists of similar, but narrower zigzag boron rows separated by hole arrays. This can explain the observed slightly smaller inter-row distance in the S2 phase (4.3 Å) than in the S1 phases (5.0 Å). Our first-principles calculation also suggests good commensuration between the χ_3 sheet and Ag(111), and the structure remains planar after relaxation, as shown in Fig. 2e. Similarly, the simulated STM image of the χ_3 sheet in Fig. 2f shows zigzag rows and alternate bright–dark protrusions along the rows, agreeing perfectly with our STM observations.

Because the atomic structures of the β_{12} sheet and χ_3 sheet on Ag(111) remain planar, without obvious vertical undulation, the 1.5 nm periodicity along the vacancy chains in the S1 phase and the dark–bright alternation in the S2 phase should correspond to the modulation of the electron density on the boron sheets. To address this question, we calculated the atomic charges of these two phases based on the Bader analysis (Supplementary Fig. 2). Inhomogeneous charge distribution is found along the boron rows in both S1 and S2 phases. Such charge inhomogeneity comes from the commensuration between the boron lattices and the Ag(111) lattice, which results in different locations of the boron atoms on the Ag(111) lattice, especially along the boron row direction.

The validity of the above models has been confirmed experimentally by measuring the atomic density of boron in the two phases. To precisely calibrate the boron coverage we used the well-known Si(111)-B-$\sqrt{3} \times \sqrt{3}$ structure as reference. Boron atoms were deposited consecutively onto the Ag(111) surface and a clean Si(111)-7 × 7 surface in the same deposition cycle, thus ensuring exactly the same flux and position of the samples. The B/Si(111) sample was then annealed to 1,000 K to obtain a Si(111)-B-$\sqrt{3} \times \sqrt{3}$ surface. Each boron atom on the Si(111) could be counted easily in the STM images, and so the boron flux could be determined precisely.

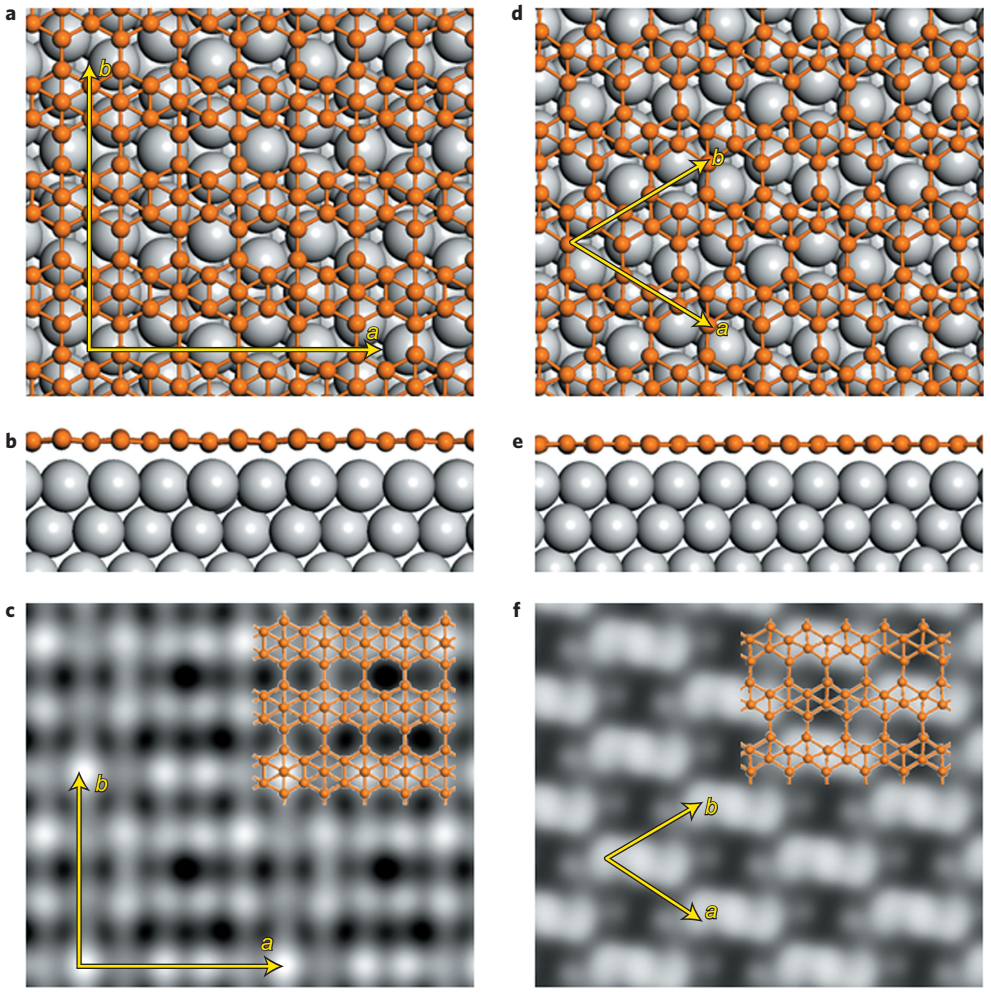

Figure 2 | Structure models of S1 and S2 phases of 2D boron sheets based on DFT calculations. a,**b**, Top and side views of the S1 model, which corresponds to the β_{12} sheet of 2D boron on a Ag(111) surface. **c**, Simulated STM topographic image of the β_{12} sheet. **d**,**e**, Top and side views of the S2 model, which corresponds to a χ_3 sheet of 2D boron on Ag(111). **f**, Simulated STM topographic image of the χ_3 sheet. Orange and grey balls in **a**,**b**,**d**,**e** represent boron and silver atoms, respectively. The basic vectors of the super cell including the Ag(111) substrate are marked by yellow arrows. Models of the β_{12} and χ_3 sheets are superimposed on their simulated STM images, which agree very well with the experiments. The striped pattern of S1 and the alternating bright–dark protrusions of S2 are both reproduced well.

The total atomic density of boron grown on Ag(111) was determined from the calibrated boron flux and the deposition time. By counting the area ratio of the S1 phase on Ag(111) in the STM images, the atomic density of boron in phase S1 was obtained. We performed experiments on samples with different boron coverages, and the calibrated atomic density of boron in the S1 phase was found to be 33.6 ± 2.0 nm^{-2}, identical to that calculated using the β_{12} sheet model (34.48 nm^{-2}), within a small range of error. The details of the above data and analysis are provided in Supplementary Section 4. On the other hand, when we annealed the S1 surface and turned it into the S2 phase, we did not observe a significant change in the total area of the islands, indicating that the boron densities in the two structures are approximately the same. This is consistent with the fact that the χ_3 sheet model has a similar boron density (31.3 nm^{-2}) as the β_{12} sheet. The above experimental facts confirm the validity of our structure models, and rule out the possibility of boron–silver alloying.

By increasing the boron coverage, the 2D boron sheets can extend in size until they spread to cover almost the entire surface (Supplementary Fig. 3). It should be noted that when the boron coverage is close to 1 ML, many three-dimenstional (3D) clusters form on the surface, which agrees with the observation in ref. 25. Because of this 3D cluster formation, it is difficult to obtain multilayer boron films. We suggest that this is because the silver–boron interface interaction is necessary to stabilize boron atoms in a 2D form. When the boron coverage exceeds 1 ML, the interface interaction will saturate, resulting in spontaneous formation of 3D boron clusters.

One of the two 2D boron phases in our study, the S2 phase, was also reported in the parallel work by J. Mannix and colleagues[25]. They observed two distinct boron phases: a homogeneous one that corresponds to the S2 phase we describe here, and a more corrugated 'striped' one that forms at very high substrate temperature (1,000 K). The S1 phase we describe here was not observed, and conversely we did not observe the striped phase in our study. Instead, under high-temperature conditions we observed the growth of 3D boron clusters (Supplementary Fig. 1d). Therefore, at least three stable boron sheets have now been observed experimentally, which agrees with the large number of energetically close phases found in theoretical predictions.

XPS study on 2D boron. The chemical bonding in our 2D boron sheets on Ag(111) was investigated by *ex situ* XPS. Figure 3a,b presents the XPS data for a typical sample of 0.7 ML pure S1 phase. Figure 3a shows the boron 1*s* signal, as well as carbon 1*s* and O 1*s* peaks, which are due to air contamination during

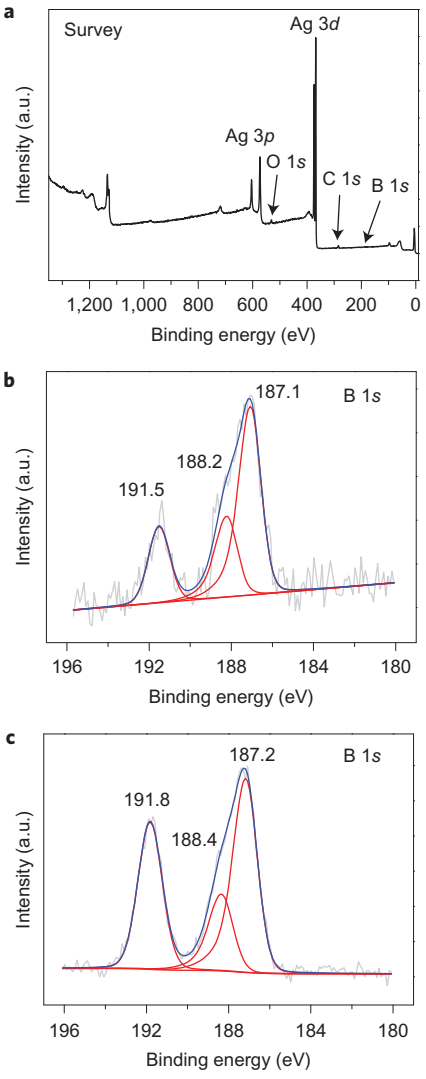

Figure 3 | XPS results for 2D boron sheets on Ag(111) after exposure to air. a,**b**, Full-scale survey (**a**) and boron 1s spectrum (**b**) of boron sheets on Ag(111) (the S1 phase) with boron coverage of ~0.7 ML. **c**, Boron 1s spectrum of boron sheets on Ag(111) with boron coverage of 1.0 ML. Three peaks can be resolved. The peak at higher binding energy corresponds to the B–O peak, and the two peaks at lower binding energy are B–B peaks. These peaks were fitted using asymmetric and symmetric Gaussian–Lorentzian functions for the B–B and B–O peaks, respectively. The Lorentzian component was fixed at 10% for all fits. A Shirley background was subtracted before peak fitting. Grey, red and blue curves correspond to original data, fitting lines and sum of fitting lines, respectively. It is evident that most boron atoms remain unoxidized in **b** (low coverage sample), and the number of oxidized boron atoms increases notably in **c** (high coverage sample).

sample transfer under ambient conditions. Three peaks can be resolved in the boron 1*s* signal in Fig. 3b, 191.5, 188.2 and 187.1 eV, indicating that there are three types of boron atom with different chemical environments. As the binding energy of the boron 1*s* peak in bulk boron is ~189–190 eV (ref. 27), the two low binding energy peaks (188.2 and 187.1 eV), which are slightly redshifted compared with the bulk value, are most probably from B–B bonds in the pristine 2D boron sheets. On the other hand, the higher energy peak (191.5 eV) implies oxidation of boron during exposure of the samples to air, in accordance with the oxidized boron peaks reported previously[28]. Note that as the boron sheet is metallic and the oxidized boron is insulating, we used asymmetric peaks to fit the two B–B peaks and a symmetric peak to fit the

Table 1 | Formation energies for free-standing and epitaxial S1 and S2 boron sheets.

	S1	S2
E_{FB} (eV per atom)	6.23	6.19
E_{EB} (eV per atom)	6.32	6.35
ΔE_1 (eV per atom)	0.09	0.16
ΔE_2 (eV Å^{-2})	0.03	0.05

E_{FB} is the formation energy per atom for the free-standing boron sheet. E_{EB} is the formation energy per boron atom for the epitaxial boron sheet. ΔE_1 is the adhesion energy of the boron sheet per boron atom. ΔE_2 is the adhesion energy of the boron sheet per unit area.

oxidized boron peak. Importantly, the measured area ratio of the B–O peak to B–B peak is ~0.23, indicating that most boron atoms remain intact. To further strengthen this point, we performed a STM experiment on the 2D boron sheets exposed to oxygen gas in different doses, and the results are shown in Supplementary Fig. 6. We found no sign of oxidation of the film at small O_2 dose. With high O_2 dose, bright spots occur at the edges of the boron sheets, but the terrace of boron remains almost intact. This experiment confirms that the boron sheets are oxidized from their edges, and the boron atoms inside the islands are quite inert to oxidation. This is why the ratio of oxidized to unoxidized boron atoms is small (0.23), even with long exposure to air. The two B–B peaks (188.2 and 187.1 eV) can be explained by the different distributions of the atomic charges in 2D boron. Interestingly, the boron atoms in our 2D boron sheets can be classified into two groups: those in the centre of the hexagonal boron rows are negatively charged, and those around the holes are positively charged (Supplementary Fig. 2). As such, the boron atoms in our 2D boron sheets have two different chemical environments, agreeing well with the two B–B peaks observed in XPS measurements.

On the other hand, the XPS data of another sample with a boron coverage of ~1 ML also shows three boron 1*s* peaks (Fig. 3c), but the area ratio of the B–O peak to the B–B peak increases to ~0.46. As the major difference between the low-coverage and high-coverage samples is the appearance of 3D boron clusters at high coverage (Supplementary Fig. 3c), we suggest that the increased B–O peak mainly comes from the oxidation of 3D boron clusters. Combined with STM experiments on the oxidization of our 2D boron sheets (Supplementary Fig. 6), we suggest that the 2D boron sheet is more inert to oxidation than the 3D boron clusters. This chemical stability of 2D boron sheets is promising for future device applications.

Formation mechanism. Previously, a large number of 2D boron sheet structures have been predicted theoretically, with competitive formation energies. However, among these models, neither β_{12} nor χ_3 corresponds to the global energy minimum[20]. To understand why we observe these two structures, we calculated the formation energies of the S1 and S2 structures, as shown in Table 1. The formation energy of freestanding S1 is 0.04 eV higher than that of S2, indicating a higher stability of isolated S1 over S2. Nevertheless, the adhesion energy of S2 (0.16 eV per atom) on Ag(111) is larger than that of S1 (0.09 eV per atom). Thus, the total formation energy for S1 (6.32 eV per atom) is actually slightly smaller than that of S2 (6.35 eV per atom). This means that S2 is thermodynamically more stable when it adsorbs on Ag(111), which agrees with the higher thermal stability of the S2 phase in our experiment. Our calculation agrees with the independent theoretical work by Zhang and colleagues, which predicted that the β_{12} structure is stable for boron on Ag(111)[26]. In addition, in a direct comparison, a recent theoretical work[29] has suggested that our two structures are more stable than the distorted triangular structure proposed in ref. 25. The 'striped phase' reported in ref. 25 is

thermodynamically less stable, and may thus require specific conditions to form. For example, careful control of the boron flux was found to be critical for the formation of this phase[25], which may explain why we did not observe it in our study.

The boron–silver interaction should play an important role in the formation of 2D boron on the Ag(111) substrate, resulting in optimal structures not necessarily corresponding to a global energy minimum in vacuum. Furthermore, the perfect commensuration of the lattice parameters of the β_{12} and χ_3 sheets with that of Ag(111) can efficiently lower the strain, favouring their formation on Ag(111). Finally, 2D boron structures with hexagonal holes in the triangular lattice can be described by the hole density η, which is defined as the ratio of hexagonal holes to boron atoms in the original triangular lattice. The β_{12} and χ_3 sheets have very close hole densities (1/6 and 1/5)[20], which explains the easy transition between the two structures on annealing.

The fact that both the β_{12} sheet and the χ_3 sheet maintain their isolated planar structures after adsorption on Ag(111) implies that the interactions between the boron sheets and the Ag(111) surface are not strong, in agreement with previous theoretical results[24]. Indeed, the calculated adhesion energy between the S1 phase and Ag(111) is 0.03 eV Å^{-2}, on the same order as the binding energy of graphite (0.019 eV Å^{-2})[30] and monolayer graphene on Cu(111) (0.022 eV Å^{-2})[31]. This implies that the S1 boron sheet could be separated from the substrate, in a manner analogous to graphene, and as also suggested by previous work[24]. The slightly larger adhesive energy (~0.05 eV Å^{-2}) for the S2 phase on Ag(111) indicates that S2 is more strongly bonded to the substrate, but still not difficult to detach. According to our first-principles calculations, the weak interfacial interaction is also reflected by the large distance between the boron sheets and the substrate (~2.4 Å), as well as by the very tiny charge transfer from Ag(111) to the boron sheet (~0.03 electrons per boron atom). Combined with the XPS and STM results, which indicate that the boron sheets are hard to oxidize, it may be possible to obtain freestanding 2D boron sheets, and construct the devices based on 2D boron in the future.

The calculated band structures of the two types of boron sheet are presented in Supplementary Fig. 7. Both boron structures are metallic, in accordance with the band structures determined in previous calculations[19,20] and our density functional theory (DFT) results on freestanding 2D boron (Supplementary Fig. 8). Scanning tunnelling spectroscopy (STS) of the 2D boron surface (Supplementary Fig. 9b) shows a prominent peak at −2.5 V (the STS results of phases S1 and S2 are similar). The local density of states (LDOS) at a bias ranging from −2 V to +2 V is relatively low, but the spectrum at a lower range of bias voltage (Supplementary Fig. 9c) shows a significant density of states (DOS) around the Fermi level, which proves that the 2D boron sheets are metallic. We also calculated the projected density of states (PDOS) of 2D boron (Supplementary Fig. 10), which gave a high *p*-band peak at −2.0 eV (−2.5 eV) for the S1 (S2) phase and a DOS distribution around the Fermi level, in good agreement with the experimental STS results.

Although the boron–silver interaction was found to be weak in our 2D boron sheets, intensive edge electronic states are indicated by the brighter edges of 2D boron islands observed in the STM images (Fig. 1a,d). STS on the edges (Supplementary Fig. 9b,c) show additional shoulders around −3.0 and −0.2 eV, and the dI/dV maps at −3.2 and −0.2 eV (Supplementary Fig. 9e,g) show most prominent bright edges, indicating the existence of edge states. Our first-principles calculations on boron nanoribbons (for details see Supplementary Section 10) indicate that the boron sheets are bonded to the Ag(111) substrate predominately through their edges, where the electron density is much higher than in the inner part of the boron sheet. Such edge interactions, as well as the resulting edge state, may play important roles in the future electronic applications of 2D boron nanoribbons.

Conclusions

Our experiments and first-principles calculations have confirmed the formation of two types of 2D boron structure on Ag(111): β_{12} sheet (independently predicted theoretically during the submission of our manuscript)[26] and χ_3 sheet. The boron sheets are quite inert to oxidation, and interact only weakly with the Ag(111) substrate. Our results pave the way to exploring boron-based microelectronic device applications. As well as Ag(111), other substrates, such as Au(111), Cu(111) and metal borides[23,24], might also be good platforms for the synthesis of monolayer boron sheets. Substrates with different interactions with boron may produce 2D boron sheets with different structures. The novel physical or chemical properties of boron sheets, such as massless Dirac fermions[22] and novel reconstruction geometries[32], may be realized in 2D boron sheets with special structures, and remain to be investigated in the future.

Methods

Experiments. The experiments were performed in a UHV chamber combining a MBE system and a low-temperature (4.5 K) STM with a base pressure of 2×10^{-11} torr. The samples were grown in the MBE chamber. Single-crystal Ag(111) was cleaned by repeated argon ion sputtering and annealing cycles. Pure boron (99.9999%) was evaporated from an electron-beam evaporator onto the clean Ag(111) substrate while keeping the substrate at appropriate temperatures. The pressure during boron growth was better than 6×10^{-11} torr. After growth, the sample was transferred to the STM chamber without breaking the vacuum. All the STM images and STS spectra were taken at 78 K, and the bias voltages were defined as the tip bias with respect to the sample. The XPS experiments were performed *ex situ* by taking the as-prepared sample out into air, and transferring it into the XPS system (ThermoFisher Scientific ESCALAB 250X with a monochromatic Al K_α X-ray source, $h\nu$ = 1,486.6 eV). The XPS instrumental resolution was 0.48 eV (determined from the Ag $3d_{5/2}$ peak). The binding energy and Fermi level were calibrated by measurements on pure Au, Ag and Cu surfaces. The software used for XPS data fitting was XPSPEAK. The XPS peaks were fitted with a mixture of Gaussian and Lorentzian functions. The ratio of Lorentzian and Gaussian components was fixed to the same value, and other parameters such as peak height and full-width at half-maximum were allowed to change. We tested different Lorentzian/Gaussian ratios, and the current one (10% Lorentzian) gave the best fitting.

Calculations. DFT calculations were performed using a projector-augmented wave (PAW) pseudopotential in conjunction with the Perdew–Burke–Ernzerhof (PBE)[33] function and plane-wave basis set with energy cutoff at 400 eV. For the S1 phase, the calculation cell contained a boron film on a five-layer $3\sqrt{3} \times 5$-Ag(111) surface. The surface Brillouin zone was sampled by a $3 \times 3 \times 1$ Monkhorst–Pack *k*-mesh. For the S2 phase, the boron film was positioned on five-layer 3×3-Ag(111) surface. The Brillouin zone was sampled by a $5 \times 5 \times 1$ Monkhorst–Pack *k*-mesh. As the PBE function usually overestimates the chemical bond length, the lattice constant of Ag(111) used in the calculations was 3% larger than the experimental value, and a vacuum region of ~15 Å was applied. All structures were fully relaxed until the force on each atom was less than 0.05 eV Å^{-1}, and the bottom two layers of silver atoms were fixed. The simulated STM images were obtained using the constant current mode based on calculated electron densities. All calculations were performed with the Vienna *Ab initio* Simulation Package (VASP)[34].

Received 17 July 2015; accepted 2 March 2016;
published online 28 March 2016

References

1. Woods, W. G. An introduction to boron: history, sources, uses, and chemistry. *Environ. Health Perspect* **102,** 5–11 (1994).
2. Albert, B. & Hillebrecht, H. Boron: elementary challenge for experimenters and theoreticians. *Angew. Chem. Int. Ed.* **48,** 8640–8668 (2009).
3. Ogitsu, T., Schwegler, E. & Galli, G. β-Rhombohedral boron: at the crossroads of the chemistry of boron and the physics of frustration. *Chem. Rev.* **113,** 3425–3449 (2013).
4. Fowler, J. E. & Ugalda, J. M. The curiously stable B_{13}^+ cluster and its neutral and anionic counterparts: the advantages of planarity. *J. Phys. Chem. A* **104,** 397–403 (2000).
5. Zhai, H.-J., Kiran, B., Li, J. & Wang, L.-S. Hydrocarbon analogues of boron clusters—planarity, aromaticity and antiaromaticity. *Nature Mater.* **2,** 827–833 (2003).
6. Aihara, J.-I. B_{13}^+ is highly aromatic. *J. Phys. Chem. A* **105,** 5486–5489 (2001).

7. Huang, W. *et al.* A concentric planar doubly π-aromatic B_{19}^- cluster. *Nature Chem.* **2,** 202–206 (2010).
8. Popov, I. A. *et al.* A combined photoelectron spectroscopy and *ab initio* study of the quasi-planar B_{24}^- cluster. *J. Chem. Phys.* **139,** 144307 (2013).
9. Sergeeva, A. P. *et al.* Understanding boron through size-selected clusters: structure, chemical bonding, and fluxionality. *Acc. Chem. Res.* **47,** 1349–1358 (2014).
10. Piazza, Z. A. *et al.* Planar hexagonal B_{36} as a potential basis for extended single-atom layer boron sheets. *Nature Commun.* **5,** 3313 (2013).
11. Castro Neto, A. H., Guinea, F., Peres, N. M. R., Novoselov, K. S. & Geim, A. K. The electronic properties of graphene. *Rev. Mod. Phys.* **81,** 109–162 (2009).
12. Geim, A. K. & Novoselov, K. S. The rise of graphene. *Nature Mater.* **6,** 183–191 (2007).
13. Wang, X. J. *et al.* Single crystalline boron nanocones: electric transport and field emission properties. *Adv. Mater.* **19,** 4480–4485 (2007).
14. Liu, F. *et al.* Metal-like single crystalline boron nanotubes: synthesis and *in situ* study on electric transport and field emission properties. *J. Mater. Chem.* **20,** 2197–2205 (2010).
15. Zhai, H.-J. *et al.* Observation of an all-boron fullerene. *Nature Chem.* **6,** 727–731 (2014).
16. Tang, H. & Ismail-Beigi, S. Novel precursors for boron nanotubes: the competition of two-center and three-center bonding in boron sheets. *Phys. Rev. Lett.* **99,** 115501 (2007).
17. Tang, H. & Ismail-Beigi, S. Self-doping in boron sheets from first principles: a route to structural design of metal boride nanostructures. *Phys. Rev. B* **80,** 134113 (2009).
18. Penev, E. S., Bhowmick, S., Sadrzadeh, A. & Yakobson, B. I. Polymorphism of two-dimensional boron. *Nano Lett.* **12,** 2441–2445 (2012).
19. Ozdogan, C. *et al.* The unusually stable B_{100} fullerene, structural transitions in boron nanostructures, and a comparative study of α- and γ-boron and sheets. *J. Phys. Chem. C.* **114,** 4362–4375 (2010).
20. Wu, X. *et al.* Two-dimensional boron monolayer sheets. *ACS Nano* **6,** 7443–7453 (2012).
21. Nagamatsu, J., Nakagawa, N., Muranaka, T., Zenitani, Y. & Akimitsu, J. Superconductivity at 39 K in magnesium diboride. *Nature* **410,** 63–64 (2001).
22. Zhou, X.-F. *et al.* Semimetallic two-dimensional boron allotrope with massless Dirac fermions. *Phys. Rev. Lett.* **112,** 085502 (2014).
23. Liu, H., Gao, J. & Zhao, J. From boron cluster to two-dimensional boron sheet on Cu(111) surface: growth mechanism and hole formation. *Sci. Rep.* **3,** 3238 (2013).
24. Liu, Y., Penev, E. S. & Yakobson, B. I. Probing the synthesis of two-dimensional boron by first-principles computations. *Angew. Chem. Int. Ed.* **52,** 3156–3159 (2013).
25. Mannix, A. J. *et al.* Synthesis of borophenes: anisotropic, two-dimensional boron polymorphs. *Science* **350,** 1513–1516 (2015).
26. Zhang, Z., Yao, Y., Gao, G. & Yakobson, B. I. Two-dimensional boron monolayers mediated by metal substrates. *Angew. Chem. Int. Ed.* **54,** 13022–13026 (2015).
27. Moudler, J. F., Stickle, W. F., Sobol, P. E. & Bomben, K. D. *Handbook of X-ray Photoelectron Spectroscopy* (Perkin-Elmer, 1992).
28. Ong, C. W. *et al.* X-ray photoemission spectroscopy of nonmetallic materials: electronic structures of boron and B_xO_y. *J. Appl. Phys.* **95,** 3527–3534 (2004).
29. Xu, S. G., Zhao, Y. J., Liao, J. H. & Yang, X. B. The formation of boron sheet at the Ag(111) surface: From clusters, ribbons, to monolayers. Preprint at http://arxiv.org/abs/1601.01393 (2016).
30. Liu, Z. *et al.* Interlayer binding energy of graphite: a mesoscopic determination from deformation. *Phys. Rev. B* **85,** 205418 (2012).
31. Olsen, T., Yan, J., Mortensen, J. J. & Thygesen, K. S. Dispersive and covalent interactions between graphene and metal surfaces from the random phase approximation. *Phys. Rev. Lett.* **107,** 156401 (2011).
32. Amsler, M., Botti, S., Marques, M. A. L. & Goedecker, S. Conducting boron sheets formed by the reconstruction of the α-boron (111) surface. *Phys. Rev. Lett.* **111,** 136101 (2013).
33. Perdew, J. P., Burke, K. & Ernzerhof, M. Generalized gradient approximation made simple. *Phys. Rev. Lett.* **77,** 3865–3868 (1996).
34. Kresse, G. & Furthmüller, J. Efficient iterative schemes for *ab initio* total-energy calculations using a plane-wave basis set. *Phys. Rev. B* **54,** 11169–11185 (1996).

Acknowledgements

The authors thank Qinlin Guo for useful discussions regarding XPS data analysis. This work was supported by the MOST of China (grant numbers 2012CB921703, 2013CB921702 and 2013CBA01600), the NSF of China (grant numbers 11334011, 11322431, 11174344 and 91121003), and the Strategic Priority Research Program of the Chinese Academy of Sciences (grant number XDB07020100).

Author contributions

K.W. and L.C. designed the experiments. B.F., L.C., Q.Z., W.L. and S.L. performed experiments and data analysis (under the supervision of K.W.). J.Z., H.L. and S.M. performed the DFT calculations. B.F., L.C. and K.W. wrote the manuscript, with contributions from all authors. All authors contributed to data analyses and discussions.

Additional information

Supplementary information is available in the online version of the paper. Reprints and permissions information is available online at www.nature.com/reprints. Correspondence and requests for materials should be addressed to H.L., L.C. and K.W.

Competing financial interests

The authors declare no competing financial interests.